Volume 17 | Number 13 | 7 July 2017 | Pages 2141–2336

Lab on a Chip

Devices and applications at the micro- and nanoscale

rsc.li/loc

ISSN 1473-0197

ROYAL SOCIETY OF CHEMISTRY

CRITICAL REVIEW

Jose L. Garcia-Cordero and Z. Hugh Fan

Sessile droplets for chemical and biological assays

Lab on a Chip

CRITICAL REVIEW

View Article Online
View Journal | View Issue

Cite this: *Lab Chip*, 2017, **17**, 2150

Sessile droplets for chemical and biological assays

Jose L. Garcia-Cordero *[a] and Z. Hugh Fan *[bcd]

Received 4th April 2017,
Accepted 23rd May 2017

DOI: 10.1039/c7lc00366h

rsc.li/loc

Sessile droplets are non-movable droplets spanning volumes in the nL-to-μL range. The sessile-droplet-based platform provides a paradigm shift from the conventional, flow-based lab-on-a-chip philosophy, yet offering similar benefits: low reagent/sample consumption, high throughput, automation, and most importantly flexibility and versatility. Moreover, the platform relies less heavily on sophisticated fabrication techniques, often sufficient with a hydrophobic substrate, and no pump is required for operation. In addition, exploiting the physical phenomena that naturally arise when a droplet evaporates, such as the coffee-ring effect or Marangoni flow, can lead to fascinating applications. In this review, we introduce the physics of droplets, and then focus on the different types of chemical and biological assays that have been implemented in sessile droplets, including analyte concentration, particle separation and sorting, cell-based assays, and nucleic acid amplification. Finally, we provide our perspectives on this unique micro-scale platform.

Introduction

Droplets are formed due to surface tension of a liquid. Because of their unique properties and size compatibility, droplets have been integrated into microfluidic devices for various applications. Generating droplets in pressure-driven flows is often called droplet microfluidics.[1–3] As reviewed in the literature,[1–3] various droplets including water-in-oil, oil-in-water, gas-in-liquid, liquid-in-gas, and double emulsion (*e.g.*, water-in-oil-in-water) can be produced in microchannels or capillaries. One unique feature of droplet microfluidics is its high-throughput: each droplet is an independent reactor.

[a] *Unidad Monterrey, Centro de Investigación y de Estudios Avanzados del Instituto Politécnico Nacional (Cinvestav-IPN), Via del Conocimiento 201, Parque PIIT, Apodaca, NL, CP. 66628 Mexico. E-mail: jlgarciac@cinvestav.mx*
[b] *Interdisciplinary Microsystems Group (IMG), Department of Mechanical and Aerospace Engineering, University of Florida, P.O. Box 116250, Gainesville, Florida 32611, USA. E-mail: hfan@ufl.edu*
[c] *J. Crayton Pruitt Family Department of Biomedical Engineering, University of Florida, P.O. Box 116131, Gainesville 32611, Florida, USA*
[d] *Department of Chemistry, University of Florida, P.O. Box 117200, Gainesville 32611, Florida, USA*

Jose L Garcia-Cordero

Jose L Garcia-Cordero is a principal investigator at the Monterrey campus of the Center for Research and Advanced Studies of the National Polytechnic Institute (Cinvestav-IPN) since October 2013. Previously, Jose was a postdoctoral fellow in the group of Prof. Maerkl at the Institute of Bioengineering of the Swiss Federal Institute of Technology in Lausanne (EPFL) and obtained a PhD from Dublin City University under the guidance of Dr. Antonio J Ricco. His research group at Cinvestav-IPN focuses on developing microfluidic platforms for single cell analysis and point-of-care diagnostics.

Z. Hugh Fan

Z. Hugh Fan is a Professor in the Departments of Mechanical and Aerospace Engineering, Biomedical Engineering, and Chemistry at the University of Florida (UF), USA. Prior to joining UF in 2003, he was a Principal Scientist at ACLARA BioSciences Inc. and a Member of the Technical Staff at Sarnoff Corp. His research interests include microfluidics, BioMEMS, sensors, cancer diagnosis and prognosis. He is a Fellow of the American Association for the Advancement of Science (AAAS) and an editorial board member of Scientific Reports and Microsystems & Nanoengineering (Nature Publishing Group).

The droplet microfluidics platform has been applied for chemical reactions, nanoparticle synthesis, various nucleic acid amplification such as polymerase chain reactions (PCR), protein expression, drug discovery, chemical/biochemical analyses, and single cell studies.[1–3] Commercialization of droplet microfluidics (*e.g.*, BioRad and Raindance) has made this technique accessible to many researchers and application scientists. A number of reviews have been focused on this topic.[1–3]

In addition to pressure-driven flows, other mechanisms such as electric and acoustic actuation have been employed to generate droplets as reviewed previously.[4] One example is to use electrowetting to control droplets on an array of electrodes, and this technique is often called digital microfluidics.[5] Just like droplets in microchannels, droplets on an open surface can move, merge, and split by sequentially applying electric potentials to pairs of electrodes.[5–7] These droplets function as nanoliter-sized vessels and have been applied for chemical and biochemical reactions, immunoassays, genomics, proteomics, and cell-based assays.[5] Acquisition of Advanced Liquid Logic by Illumina in 2013 suggests the huge potential of this technique for next generation DNA sequencing.

While these mobile droplets possess unique properties and have been exploited for various applications, non-mobile droplets offer their distinctive advantages. Sessile droplets are emerging as a platform capable of competing with microplates in terms of versatility and simplicity of operation.

Sessile droplets are non-movable droplets, typically in volume ranging from 0.1 nL to 10 μL, which is similar to the volume in high-density microwell plates. Droplets can be confined in patches of different surface energy than the rest of the substrate. The sessile droplet platform can be regarded as a microplate without walls. As a result, increasing the throughput to 6144 (4 × 1536) microwells or higher could be much easier to realize. However, compared to the microwell platform, sessile droplets exhibit interesting physical phenomena that have been exploited to improve assay sensitivity, reduce total assay volumes, decrease the number of assay steps, and lessen the dependence on sophisticated instrumentation. For example, internal convection flows generated during evaporation can mix solutions without the need of any external instrumentation,[8] natural evaporation by itself has been harnessed to separate particles based on size,[9] and the whole genome from a single cell has been amplified inside a droplet.[10] In addition, sessile droplets could open the door to other interesting applications in high-throughput format, not capable with a conventional microplate.

In this review, we introduce the readers to these and other emerging applications of sessile droplets, including cell culture assays, enzymatic assays, nucleic acid amplification, analyte concentration, drug screening, and diagnostics. This review is structured in seven sections. In the first section, we discuss the reasons for the popularity of microtiter plates in laboratory, industrial, and clinical settings, and elaborate the challenges of this platform that could be addressed by sessile droplets. Next, an introduction to the physics of sessile droplets is presented for better understanding of their applications. The following five sections cover the various applications of sessile droplets in chemical and biological assays. Finally, we offer our perspective on the future of this unique sessile-droplet-based platform.

An alternative to microtiter plates

The microtiter plate is a platform that essentially contains tens or hundreds of microliter-sized test tubes. The microplate was invented in 1951 by Gyula Takátsy.[11] Since then, it has become an essential tool in most of research, industrial, and clinical settings, and for that matter in most branches of the life sciences. A recent survey reported that the top applications of microplate technology are cell biology, assay development, biomarker research, biomolecule concentration measurements, PCR setup and cleanup, and bioassay validation.[12] With so many applications for a simple technology one must wonder why the microplate has become so successful and so permissive. One could argue that over time it became a very popular tool in clinical, industrial and academic laboratories and therefore adopted as the *de facto* industry standard.[13] Indeed, the market for microplates supplies and instrumentation is expected to reach US $6.5 billion by 2022,[14] 4 times higher than in 2009.[11] The same survey reported that the top reasons to use microplate technology are to automate repeatable tasks and to ensure reproducible results; while the top factors looked for when purchasing microplate technology include flexibility, accuracy, and reliability.[12] We believe that its simplicity of use, its versatility to be employed in a variety of assays, and reproducibly, can account for the microplate past, present, and future success, and that any new technology looking for replacing microplates must compare against these metrics.

One crucial advantage of the microplate technology is its ability to operate using only a pipette, which is useful in research laboratory settings, and it can also be integrated into liquid-handling robotic stations and thus be valuable in industry.[8] This applies to the different types of assays performed in the life sciences, whether it is for culturing cells, performing immunoassays, screening for small molecule drugs, or running PCR. It is difficult to encounter other platforms with similar flexibility.

Another advantage of microplates is that they can be made of different plastics—from commonly employed polystyrene to acrylic, polypropylene, and polycarbonate—using well established mass-production techniques; thus their manufacturing is inexpensive and straightforward. For different optical readouts, the microplate can be made in black or white. And for different bioassay applications, it comes in variety of formats from 96 to 1536 wells, capable of holding from 200 μL down to less than 1 μL. Formats commonly employed in most academic labs are 96- and 384-well plates, while the low-volume 384- and 1536-wells plates are the

preferred platform in industry.[15] Working with smaller volumes offers several advantages, including (1) less consumables and lower sample/reagent consumption, which translate into cost savings; (2) higher number of samples processed in parallel, which translates into faster turnaround time; (3) generation of more and better quality data; and (4) reduction of space requirements.[13] These advantages are especially important for drug discovery.[15] However, working with smaller volumes faces difficulties on different fronts, including mixing, evaporation, and fabrication.

Effective mixing can produce consistent and reproducible results that lead to better assay statistics, reduce false positives, facilitate assay miniaturization, reduce reaction times, and improve compound solubilisation.[16] However, for plate densities higher than 384 wells, complete and effective mixing represents a challenge, given the viscosity and volatility of some liquids. For example, complete mixing of a 50 μL solution in a 384-well plate can take up as long as 50 min with vigorous orbital shaking, not much different from mixing by diffusion.[17] Although other contact or contact-free

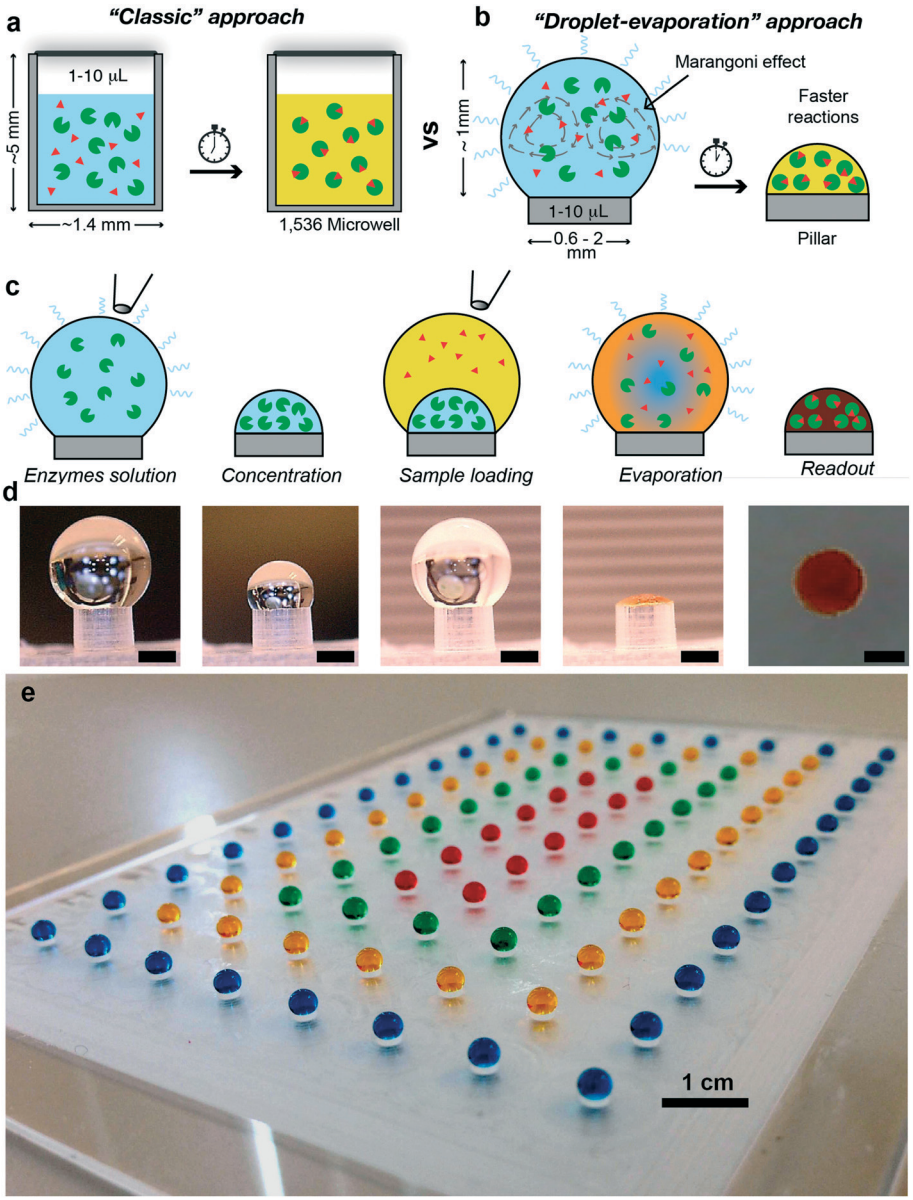

Fig. 1 The microwell plate *vs.* the sessile droplet. (a) Microwells are effectively test tubes in which assays occur. They are commonly sealed with a plastic foil to prevent evaporation. A well from a 1536 microplate can hold a volume of up to 10 μL. (b) By comparison, the sessile droplet platform can harness evaporation to drive reactions and thus increase assay sensitivity and reduce assay times. (c) Example of a colorimetric assay in a sessile droplet. An enzyme solution is deposited on a pillar and the solvent is evaporated. A sample is loaded over the concentrated enzyme. Evaporation mixes both sample and enzyme to initiate the assay. Color intensity of the droplet is proportional to the analyte concentration. (d) Actual photos of the colorimetric assay for glucose detection. Each black scale bar represents 500 μm. (e) Photograph of a droplet array in the same size of a 96-well microtiter. Adapted with permission from ref. 8. Copyright 2016 American Chemical Society.

mixing technologies exists, such as those using acoustic forces, centrifugation, sonication, or magnetic stirring, they have their own shortcomings:[8] some of them being invasive, can damage cells, are expensive and not readily available in most laboratories, lack automation compatibility, among others.[16] Another issue reported is that some of these mixing technologies cause liquids to move, jump, or wick the wells and therefore plates have to be sealed to prevent contamination,[16] but sealing may interfere with downstream processes. It is clear that there is no one-size-fits-all answer to mixing solutions in high-density microplates but mixing has become a major hindrance.

Working with small volumes also poses the problem of evaporation, which prevents certain assays from scaling down to nanoliter volumes.[18] This problem can be solved by working in high-humidity environments or overlaying the wells with a plastic or aluminum foil; however, the foil could interfere with successive steps. Another issue in small wells is the high surface-to-volume ratio, which can increase reagent adsorption and stability. Finally, the higher the well density the higher the price: a 1536-well plate can be 4 times more expensive than a 384-well plate, even though they have the same footprint and consume the same amount of plastic. Reports of 3456- (1 μL) and 9600-well plates (0.2 μL) have surfaced[13] but they are not commercially available from major vendors.

Our recent work[8] has demonstrated that sessile droplets can become an alternative to the microwell plate and solve some of these issues related to mixing, evaporation, and fabrication complexity, as shown in Fig. 1a and b. We use it as an introductory example to illustrate the advantages offered by sessile droplets such as faster reaction due to mixing resulting from the Marangoni effect (to be explained later). In this work, droplets rest over plastic pillars fabricated with a regular milling machine; the droplets remain pinned to the edge of the pillars for the duration of the assay (Fig. 1c and d).[8] A solution of enzymes is first concentrated by letting solvent to evaporate. Next, a droplet containing an analyte of interest is placed on top of the concentrated enzyme. A recirculation flow emerges as the droplet evaporates that help mix the sample with the enzymes. By harnessing evaporation to mixing, we showed that the detection of glucose and proteins from 1 μL samples was faster and more sensitive than a droplet that does not evaporate.[8] Such an assay can be implemented in the format of 96-pillar array, as shown in Fig. 1e. Over the next section we will briefly review the physics of droplets, understand how flows are generated inside a droplet, and examine the different applications that have emerged from this and other phenomena.

Physics of droplets and evaporation

In this section, we briefly discuss important concepts of sessile droplets that are useful for understanding the contents covered in this review. Those readers who are looking for more details are advised to read a handful of reviews covering the fundamental physical aspects of droplets.[19–21]

In general, a droplet assumes a spherical cap shape when placed on a substrate as shown in Fig. 2A, although large-volume droplets can sag under gravity. The radius, r, and height, h, of this spherical cap are defined by the physical properties of the solution and its interaction with the substrate. The perimeter of the wetted area on the substrate is referred as the contact line. Droplets of different solutions deposited on identical substrates will behave differently, with behaviors ranging from spreading out, to partial wetting, to a non-wetting state, as shown in Fig. 2B. This behavior also occurs for the same liquid deposited on different substrates. This wetting is quantified by measuring the contact angle, θ: the angle formed at the interface between the substrate, the liquid, and the air (*i.e.* the three-phase boundary) and can range from 0° to 180°. The equilibrium contact angle is given by the Young's equation: $\gamma_{lv}\cos\theta = \gamma_{sv} - \gamma_{sl}$, where γ_{lv}, γ_{sv}, γ_{sl}, represents the liquid–vapor, solid–vapor, and solid–liquid interfacial tensions, respectively.[22]

Unless the vicinity of a sessile droplet is saturated with the vapor of the liquid, it will unavoidably start drying out, generating fluid motion instantaneously inside the droplet.[23] The evaporation rate of a droplet is influenced by the interdependent and dynamic properties of the liquid (viscosity, surface tension, volatility), the substrate (surface material, thickness, thermal conductivity, wettability, and roughness) and its surroundings (relative humidity, temperature, and pressure).[24] For example, the drying time of a typical droplet with height-to-radius ratio of 0.5 can range from ~200 s for ethanol (a volatile liquid with vapor pressure of 5.95 kPa) to ~3 h for hexanol (non-volatile, 0.124 kPa).[19]

In general, when the contact angles is less than 90°, the evaporation of a droplet follows a two-stage process, often called the constant contact radius mode.[25] In the first stage, the contact line is pinned to the substrate and the contact angle and drop height decreases as it dries out. The edges of the droplet evaporate at a higher rate than in the center, so to maintain the contact line pinned, solvent must flow radially outward to the edges to compensate for this loss of liquid—assuming a zero shear stress on the free surface of the droplet.[25] This radial fluid flow occurring inside a droplet is known as capillary flow. If colloids are present in the liquid, they are carried by the capillary flow to the contact line, where they start to aggregate leaving a distinct coffee-ring stain (although the coffee-ring effect is familiar to anyone who has observed a drop of coffee dry, it was not until 1997 that Deegan and coworkers developed a theoretical framework to explain it[26,27]). The second stage happens when the droplet reaches a critical contact angle (2–4°) and the contact line starts to recede. More than 80% of the initial volume is lost during this stage.[28]

Other evaporation modes exist. For contact angles larger than 90°, the initial stage of evaporation is dominated by a constant contact angle and a receding contact line. A mixed

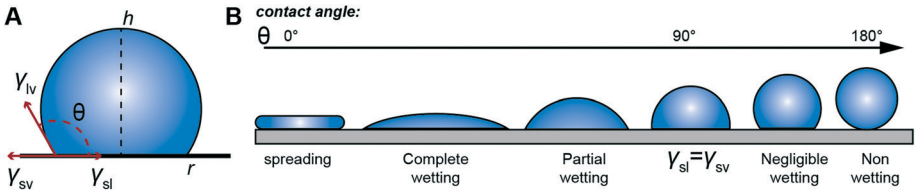

Fig. 2 (A) A droplet adopts a spherical cap forming a contact angle θ at the intersection of the liquid–solid interface (with interfacial tension at γ_{sl}) and the liquid–vapor interface (with interfacial tension at γ_{lv}). (B) Illustration of the behaviors of a droplet placed on substrates with different surface energies. Small contact angles (<90°) result from high-wettability while large contact angles (>90°) result from low-wettability.

mode consists of a combination of both modes with a simultaneous decrease in both the contact area and the contact angle.[23]

Due to the heat loss during the phase change, the evaporation process creates differences in temperature across the surface of the droplet that, in turn, produces surface tension differences along the droplet free surface.[29] This surface tension gradient can also be produced by a surfactant concentration gradient or by temperature differences between the substrate, the droplet and its surroundings.[30] This Marangoni stress induces a recirculating flow (Fig. 3) whose magnitude is a function, in part, of the droplet height and the contact angle; the taller the droplet and the higher the contact angle the faster the velocity of the recirculating flow.[30] In fact, Marangoni flows can suppress the coffee ring effect and carry colloids to the center of the droplet,[29] although they can also coexist with capillary flows.[31] This Marangoni flow, as we will see in later sections, has interesting applications for bioassays.

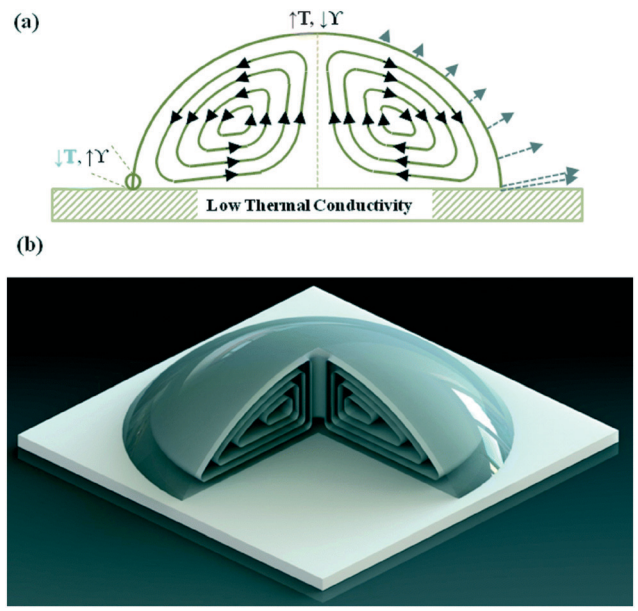

Fig. 3 (a) Recirculating flows, also called Marangoni flow, are produced by surface tension gradients (γ) and temperature gradients (T) across the droplet surface. (b) A 3D rendering of a droplet shows radial symmetry of the Marangoni flows. Reproduced from ref. 31 with permission from The Royal Society of Chemistry.

Sample enrichment *via* droplet evaporation

Detecting very low concentrations of analytes in a small volume sample is one of the major challenges in sensing. Strategies to tackle this issue involve the development of highly sensitive sensors or the elaboration of methods to concentrate analytes into a small volume before delivering to a sensor. Sample pre-concentration has become one of the first steps in many chemical and biological assays.[32] Concentration of molecules is often carried out by centrifugation, electrophoresis, western blots, chromatographic techniques, membrane dialysis, and solid-phase extraction, among others.[32–35] These techniques are well established in laboratory settings but sample processing generally starts with large volumes (*e.g.*, a few mL). Although most of these techniques have been miniaturized into microfluidic devices, there is still an unmet need for simpler methods to concentrate molecules that do not rely on external equipment.

One of the common applications of droplets is for concentrating analytes. Letting a droplet evaporate increases the analyte concentration, with the caveat of increasing the concentration of other molecules such as contaminants present in the sample. For this strategy to be exploited to its full potential, the footprint of the initial droplet (*i.e.*, the contact line) ideally should be in a size about the area occupied by a detection element (*e.g.*, a sensor). This strategy in principle could be applied to any type of samples.

Most blood proteins used for diagnosing diseases are found in very low concentrations (aM to pM).[36] While surface-based biosensors are reaching exquisite sensitivity, even at the single molecule level,[37] it is still challenging and time-consuming to deliver the analytes in highly diluted samples (<fM) to these biosensors, as most strategies are limited by the diffusion of the analytes to the sensor surface,[38–40] regardless of the sensor sensitivity.[41] Imagine a droplet is placed over a surface containing a small sensor: after evaporating a solution, its volume is reduced, and the concentration of the analyte increased, thus reducing the traveling distance of an analyte to the sensor area, thereby overcoming the diffusion limit. For this approach to work, the area enclosed by the contact line of the droplet must overlap with the sensor area for the duration of the assay (as the droplet evaporates), ensuring that analytes are not absorbed to other areas of the surface. This is possible by creating a super-

hydrophobic surface so that any liquid placed over the surface occupies, from the beginning of the experiments, the smallest surface area possible.

Fabrizio *et al.* demonstrated this approach,[38] as shown in Fig. 4A–C. They created a super-hydrophobic surface (contact angles 160–170°) using silicon micropillars. A 20 μL droplet, which initially covers a contact area with a diameter of 1.2 mm, is evaporated until it collapses into an area of a few square micrometers. They were able to detect 100 molecules of rhodamine with an initial concentration of 10 aM. Detection of a single lambda DNA molecule from a 3-μL droplet with an initial concentration of 1 aM was also reported. Using a single embedded plasmonic nanosensor on a micropilllar array they were able to detect the Raman spectra of ~5 molecules of lysozyme in 160 nL with an initial concentration of 1 fM (containing a total of ~100 molecules). A similar approach was employed to concentrate two estrogen receptor isoforms over the tips of SU8 pillars where the proteins formed stretched fibers upon evaporation. These fibers containing protein isoforms were studied using Raman spectroscopy and synchrotron X-ray diffraction.[42]

For higher sensitivity, each pillar can be potentially transformed into a single SERS sensor by decorating the pillar's tip with silver nanoparticles aggregates[37,44] (SERS or surface-enhanced Raman spectroscopy is label-free and highly specific technique used to detect single molecules[37]). Interestingly, the same pillars give rise to a super-hydrophobic surface, on which a 10 μL droplet initially occupied an area with

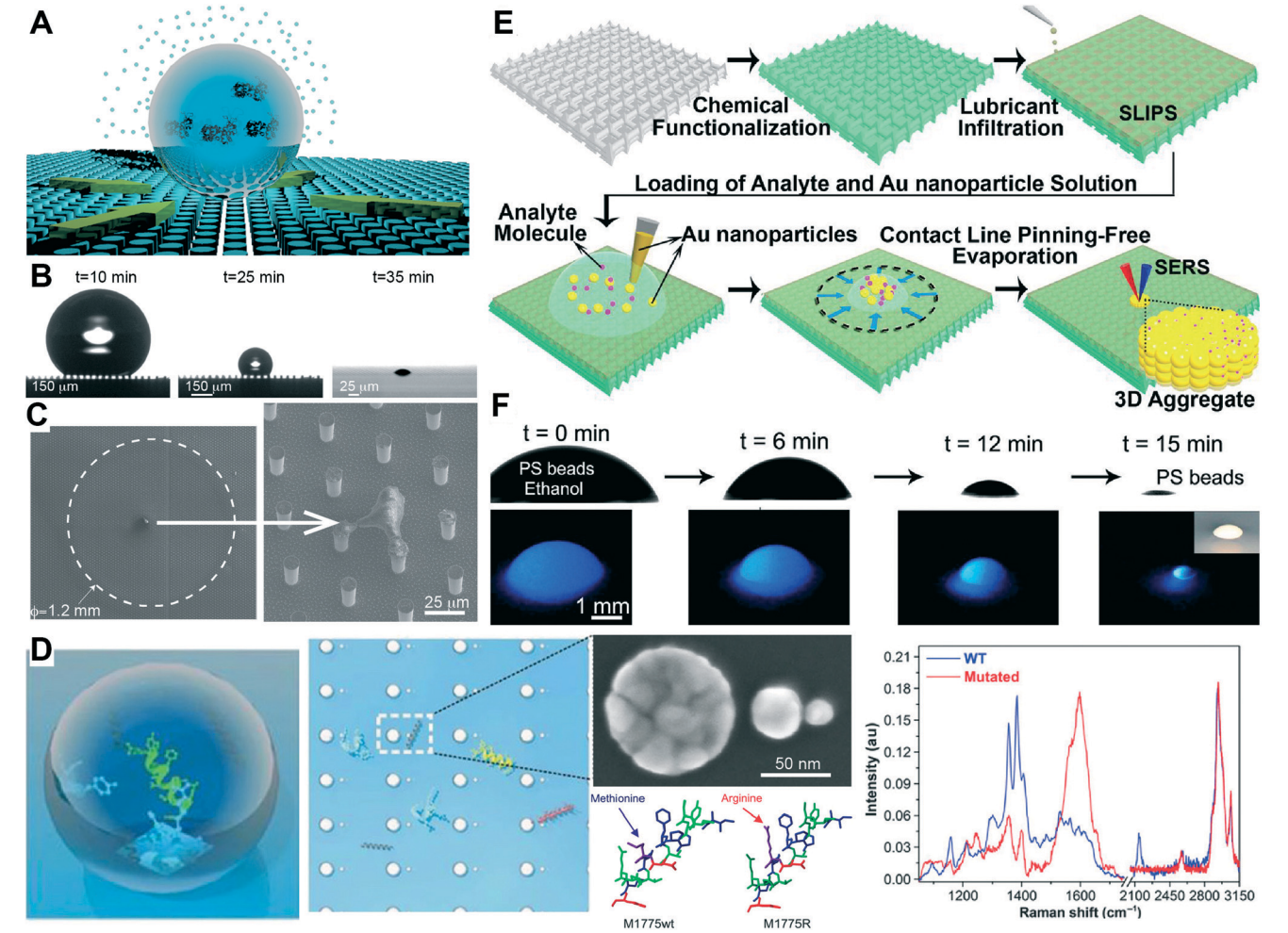

Fig. 4 Analyte concentration as a result of droplet evaporation. (A) A 3D rendering of a droplet placed on a silicon pillar array. (B) As the droplet evaporates its volume becomes smaller. The silicon pillars do not allow the pinning of the droplet, keeping the contact angle and shape of the droplet constant. (C) The droplet collapses to a region of ~25 μm from an initial contact diameter of 1.2 mm. Reprinted with permission from Macmillan Publishers Ltd: Nature Photonics,[38] copyright 2011. (D) A mixture of peptides is placed on an array of gold nano-antennas. After the droplet evaporates, some of the peptides are co-located on the surface of the nano-antennas. Raman spectra obtained from each of these hotspots can solve the molecular composition of molecules, even for peptides that differ by only one amino acid. Adapted from ref. 43 (E) A porous surface is infused with lubricant, which provides a free-pinning substrate for almost any solution. Gold colloids are mixed with the analytes and deposited on the surface. As the droplet evaporates, the contact line recedes until it collapses into a 3D aggregate. This aggregate is used for SERS detection. (F) The process is exemplified by a solution of polystyrene (PS) beads dispersed in ethanol. After 15 min., all the beads have concentrated onto a single spot. Reproduced from ref. 39, copyright 2016 Proceedings of the National Academy of Sciences.

a diameter of 1.2 mm, but upon complete evaporation the droplet residues occupied an area of only a few pillars (about 40 μm), an area ~1000 times smaller.[44] With this arrangement it is possible to increase the concentration >100-fold of an analyte.[37] In an effort to simplify the fabrication of SERS substrates, Yang *et al.* replaced the micro-pillars array with a polystyrene-silver (PS-Ag) Janus particle array, which not only presented a high hydrophobicity (150°) but the silver surface also acted as a SERS substrate. Using 10 μL water droplets they were able to detect rhodamine 6G, poliovirus RNA polymerase, and a virus at concentrations of 1 pM, 1 nM, and 1 fM, respectively.

One problem with this micropillar array is that their fabrication is time-consuming and expensive, and may not be necessary if most of the surface where the droplet sits is properly functionalized, or if the concentration is high enough that a few molecules would overlap on the surface sensor once the droplet dries out. For example, Fabrizios' group created an array of 10 × 10 silver plasmonic nano-structures, dubbed self-similar chains, which acted as hotspot regions for Raman spectroscopy,[43] as shown in Fig. 4D. A droplet containing a mixture of peptides extracted from the BRCT domain of the BRCA1 protein (which gene has been associated to breast and ovarian cancer) was evaporated on the nano-structure array until it dried out. Performing multicomponent mixture analysis on the Raman spectra obtained from each hotspot allowed to discriminate between 25 different peptides, and most astonishingly, detect a single mutation in a 16 amino-acid peptide.[43]

The samples on these experiments used water as a solvent, but real samples contain a variety of matrices, from blood, urine, to non-aqueous solvents. The breakthrough came from a surface that would not foul under any of these matrices. Slippery liquid-infused porous surface (SLIPS)[45] is a substrate patterned with nano/microstructures that are permeated with a lubricant fluid, instead of air or liquid as in the case of the micropillars. SLIPS eliminates the pinning of the contact line for almost any liquid, including blood and crude oil, so that the droplet would collapse into a small area. In other words, hardly any analyte would be lost to the surface and therefore the collapsed droplet would contain essentially all analytes. Using SLIPS, droplets of a 50–100 μL of sample are mixed with gold nanoparticles and upon complete evaporation the same metallic colloids act as a SERS substrate, as shown in Fig. 4E and F. The authors demonstrated the detection of different biomolecules (dyes, nucleic acids, and proteins) at subfemtomolar concentrations in either aqueous and non-aqueous solvents, an impressive feat for the droplet platform.[39]

Label-free non-optical detection techniques can also benefit from droplet evaporation.[41,46] For example, non-faradaic impedance spectroscopy was employed to detect DNA molecules in deionized water.[41] Solutions of 3 μL droplets were evaporated on texturized super-hydrophobic electrodes and showed a limit of detection of 10 aM, an improvement of 5 orders of magnitude compared to previously reported impedance sensing approaches.

Droplet evaporation has also been employed for the detection of organic and inorganic molecules and as a concentration step for other type of assays. Yanagimachi *et al.*[47,48] showed that heavy metal ions could be concentrated through anodic stripping voltammetry, in which heavy metals are first reduced and deposited on a working electrode. The authors found that the higher the volume of a droplet (5–20 μL) the higher sensitivity—at the expense of longer evaporation times.[47,48] Using the same approach, enzymes can also be concentrated and immobilized on an electrode by evaporation, resulting in improved sensitivity.[49] Hayes and colleagues demonstrated that evaporated droplets can be analyzed by matrix-assisted laser desorption ionization (MALDI) and improve sensitivity by a factor of 5 compared to a standard MALDI plate.[50]

Similarly, Khine and co-authors demonstrated that evaporation of a droplet on a super-hydrophobic plastic substrate enhances 16 times the detection sensitivity of proteins than without evaporating the solution.[51] They also showed detection of proteins in urine samples by adding colorimetric assay reagents to the evaporated droplet.

As noted in these early reports, one problem of these strategies is the accompanying increase in the concentration of other molecules that could interfere with the sensing technique. One possibly solution is to remove some of the contaminants prior to depositing the droplet over the sensor. Another solution is to use a permeable selective membrane that only allows the diffusion of the analyte of interest to the sensor. This strategy was employed to detect heavy metals.[48] Although the larger the volume the longer it takes to evaporate, it is possible to heat the surface or use air currents to accelerate the evaporation rate.

These results highlight how an evaporating droplet can deliver analytes to a sensor. Although in some cases the substrate has to be crafted accordingly to produce a superhydrophobic surface, this may not be necessary for every application if one is only looking to gain at least an order of magnitude on sensitivity. In the future, one could imagine a substrate with two or more sensors, and by carefully tailoring the surface properties, direct some portion of the sample to each sensor area.

Coffee-ring effect for microparticle separation

Separation and sorting of cells and microparticles is an essential step in many biomedical and environmental applications.[52,53] Sorting can be based on physical properties such as size or density, and applications include the separation of the different types of blood cells, sorting of tumor cells from normal cells, or isolation of bacteria from a polluted sample.[53] Macroscale techniques for separating cells include centrifugation and fluorescence-activated cell sorter (FACS), but they require very bulky and expensive equipment. Dozens of different microfluidic techniques have been developed to discriminate cells based on different properties,[52,53] but most

of these devices are fabricated using sophisticated lithography techniques and their operations are labor intensive with external accessories (*e.g.*, syringe pumps or pressure sources) that have limited their widespread use outside microfluidics research groups. Hence, there is still an unmet need for low-cost and simple methods for the separation of microparticles.

One of the most astonishing applications of an evaporating droplet is precisely the separation and sorting of particles without necessitating any external equipment or requiring microfabrication techniques. Induced capillary flows in an evaporating droplet transport particles towards the contact line (*i.e.*, rim) where they are trapped at positions where their diameter matches the height of the liquid meniscus. At the early stages of evaporation, the magnitude of this drag force—produced by the capillary force—on microparticles has been calculated to be on the order of 10^{-10} to 10^{-12} N.[54–56] As the droplet evaporates, the particles start forming a series of concentric ring structures, with the largest and smallest particles occupying the innermost and outermost ring, respectively,[57] as shown in Fig. 5A and B. Towards the end of the evaporation process, as the contact line recedes, the surface tension force drags the microparticles to the center of the droplet.[55,56]

Separations of microspheres and nanoparticles of different diameters in one droplet were reported by Wong *et al.*[9] and Monteux and Lequeux.[57] The staggering demonstration was to separate antibodies, bacteria and lymphoma cells in three concentric rings,[9] shown in Fig. 5C. Also, with the use of dielectrophoresis (DEP), Jung and Kwak reported the separation of red blood cells and bacteria on a sessile droplet.[54] A 3D microtrap array suspended on a bed of micropillars was shown to filter microbeads smaller than the pillars gap size, while bigger microbeads were docked on the microtraps as the droplet evaporated.[58] More recently, BSA (<7 nm) and nanoparticles (<500 nm) were also shown to form a double ring; however, it was noted that the electrical charge of the nanoparticles and their interactions with biomolecules can greatly affect the ring formation.[59] Separation of larger microparticles (50–200 μm) has also been achieved by exploiting Marangoni currents generated during the evaporation of a droplet at high temperatures.[60] One caveat of this method is that it only works with low volume fractions (<0.05%) and low contact angles.[9,54–57] Although these are only a few examples, the field is ripe for more applications in different areas.

Other applications of the coffee-ring effect

As we noted in the previous section, the coffee ring can separate and sort microparticles, and these particles or molecules are concentrated in the form of concentric rings at the edge of the droplet. The width of these annuluses is proportional to the particle concentration and to the droplet radius. This was the case for the detection of small fluorescent molecules (between 300–450 Da), in which the width of the annulus was found to be proportional to its concentration, making possible the detection of femtomole levels in a 0.1 μL droplet.[61–63] Wen *et al.* demonstrated that fluorescent aptamer-analyte complexes in serum and diluted blood could be concentrated at the coffee ring interface, yielding fluorescent intensity signals 40 times greater than from a liquid droplet,[64] as shown in Fig. 6A. A solution is initially mixed for 30 min with antithrombin aptamer, which fluoresces upon binding to its target. 1 μL of the solution was allowed to dry, causing the α-thrombin-aptamer complexes to migrate to the edge and form a coffee ring that results in an increased assay sensitivity. They reported the limit of detection (LOD) of 54 pM for serum and 105 pM for diluted blood. These examples show that by just evaporating a sample and letting the analyte accumulate in the coffee ring, the signal intensity can be greatly enhanced by at least an order of magnitude. However, the optimization of several conditions, including temperature, pH, and viscosity, are required, indicating that tweaking is needed to apply the same technique to other types of molecules.

Most molecules are not fluorescent so other techniques are required to identify and quantify them. Raman spectroscopy

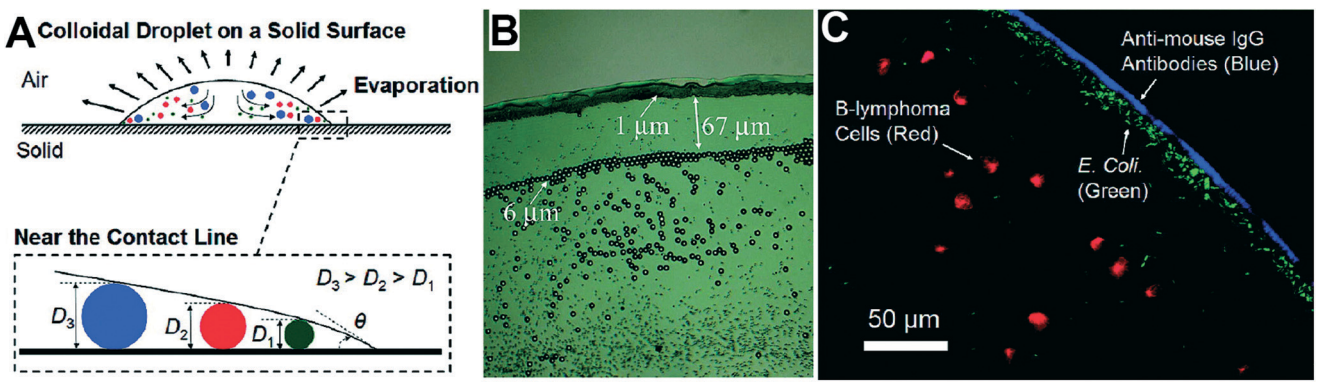

Fig. 5 Separation of particles employing the coffee-ring effect. (A) As a droplet evaporates, colloids are transported to the edge of the droplet, forming bands in which the smallest particles are localized closest to the contact line while the biggest particle are located further from it. Adapted with permission from ref. 9. Copyright 2011 American Chemical Society. Examples of (B) separation of polystyrene microbeads of different diameters and (C) sorting of bacteria, cells, and antibodies. Adapted with permission from ref. 54. Copyright 2007 American Chemical Society.

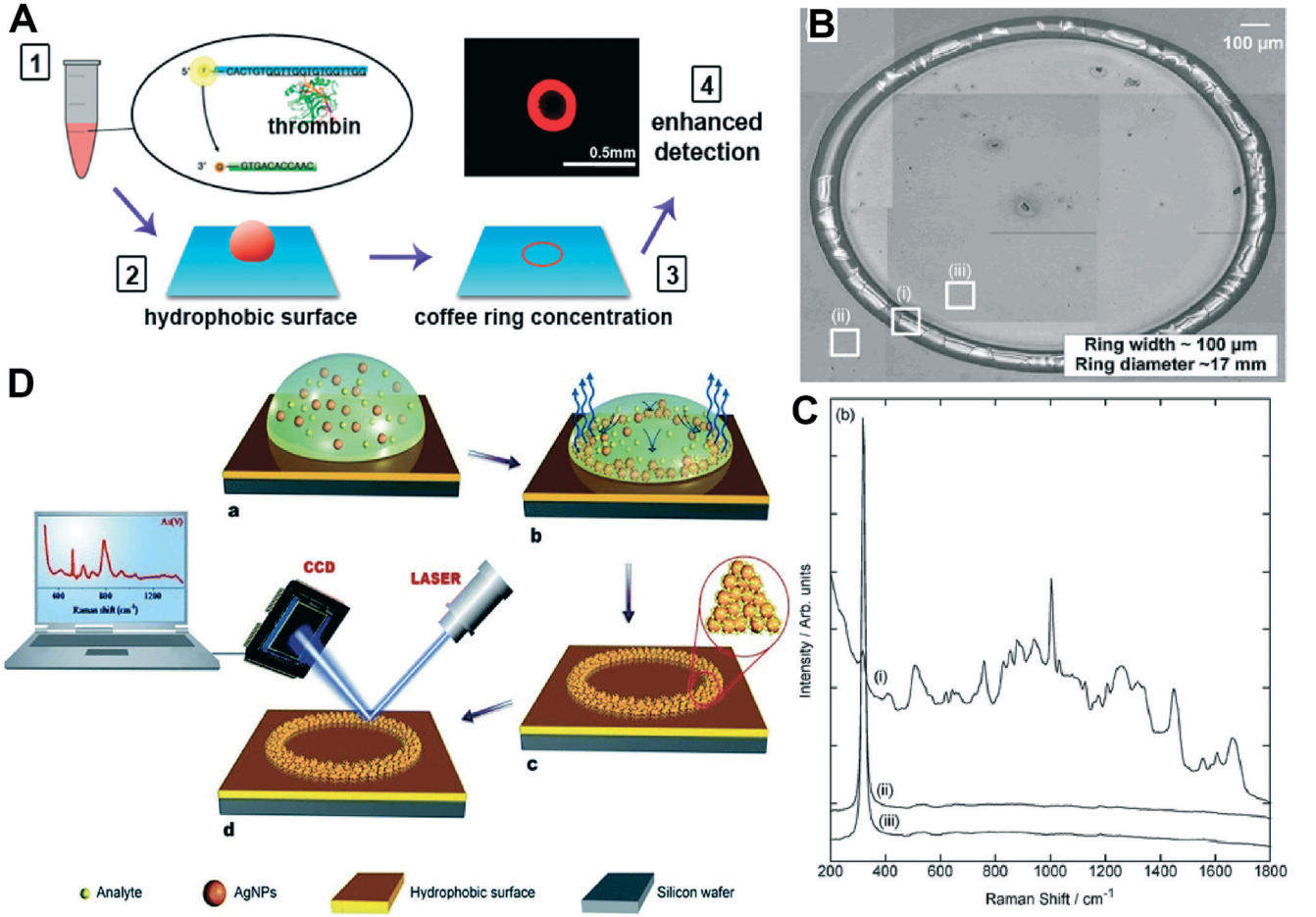

Fig. 6 Coffee ring effect for concentration and detection of analytes. (A) A drop from a solution containing α-thrombin and a fluorescently labeled anti-thrombin aptamer is placed on a hydrophobic surface. Upon evaporation, the molecular complex is concentrated on the coffee ring, which enhances the assay sensitivity. Reprinted with permission from ref. 64. Copyright 2013 American Chemical Society. (B) Ring-pattern formation of lactoferrin, a protein found in tears. (C) Raman spectra obtained at three marked locations in (B) and only one on the dried ring (i) showed the spectrum whereas other two spots (ii and iii) had undetectable Raman shift. Reproduced from ref. 67 with permission from The Royal Society of Chemistry. (D) (a) A droplet containing an analyte and silver nanoparticles is deposited on a hydrophobic substrate. (b and c) As the droplet evaporates, the nanoparticles start self-assembling on the edge of the droplet, trapping the analyte. (d) Analytes are detected by confocal Raman spectroscopy. Reproduced from ref. 70 with permission from The Royal Society of Chemistry.

is a technique that can identify molecules based on their vibrational modes.[65] Although every molecule has a unique Raman spectrum, the intensity of the Raman signal is orders of magnitude smaller than fluorescence,[65] and thus sample enrichment would be very useful. Raman spectroscopy was used to analyze the contents of coffee ring deposits, detecting several molecules in volumes ranging from 1–10 μL with concentrations as low as 1 μM,[66] as shown in Fig. 6B and C. This technique, also known as drop coating deposition (DCD) Raman, has allowed the identification of different biomolecules on Teflon-coated stainless steel. The molecules identified by DCD-Raman include glucose, insulin, lysozyme, lactoferrin, albuminum, bacterial toxins, and liposomes.[34,66–68]

The Raman scattering can be increased when molecules are in close proximity to a roughen noble-metal surface;[65] this process is known as surface enhanced Raman spectroscopy (SERS). SERS was combined with DCD to diagnose the causes of adenoviral conjunctivitis in 2 μL sample of human tears.[69] The coffee ring was employed to self-assemble silver nanoparticles at the edge of an evaporating droplet, which then served as SERS hot-spots to detect organic and inorganic molecules,[70] as shown in Fig. 6D. Another study has been carried out to determine the size of a coffee ring structure as a function of the initial droplet diameter, nanoparticle size and concentration, and surrounding humidity,[71] which could be important to take into account when designing new bioassays based on the coffee ring. Coffee rings as small as 10 μm can be formed with 100 nm particles.[71]

Detection of biomarkers is critical in the diagnosis of diseases. Current gold standard techniques include ELISA, western blots, and lateral flow assays; however, these techniques involve time-consuming sample processing, costly laboratory equipment, and skilled personnel.[64] One major trend in diagnostics is to develop low-cost, robust, and simple-to-use tests.[72] This requires working with sample and reagent volumes as small as possible and minimizing the reliance on

external instrumentation. In fact, the ideal test should produce a detectable signal in a short period of time, preferable with a signal that is easy to interpret. Harnessing the coffee-ring effect can offer some of these characteristics. As a proof-of-concept to detect malaria, Haselton and colleagues developed an assay based on the change in color of the coffee-ring pattern and on the deposition of particle aggregates in the center of the droplet. They employed a mix of fluorescent 1-μm microparticles of different colors (green or red) and magnetic nanoparticles.[73] The magnetic nanoparticles and the green microparticles were functionalized with a ligand [Ni(II) nitrilotriacetic acid or Ni(II)NTA] that induces particle aggregation in the presence of the analyte while the red microparticles were nonreactive. When the analyte is not present, both microparticles migrate to the edge of the droplet forming a yellowish coffee ring while the magnetic nanoparticles are pulled to the center of the droplet by a magnetic field. When the analyte is present, magnetic nanoparticles and green microparticles start to aggregate giving rise to a green disk at the center of the droplet while the edge of the droplet (coffee ring) becomes more reddish. The fluorescent intensity of the green disk is proportional to the amount of analyte present, as shown in Fig. 7A and B. Using this antibody-free approach, they detected poly-L-histidine, a surrogate of a malaria biomarker, *pf*HRPII, to concentrations as low as 200 nM.[31] A variant of this method was later reported, in which all microparticles were replaced with 1 μm gold-plated polystyrene spheres (AuPS) functionalized with Ni(II)NTA.[72] A 1-μL solution

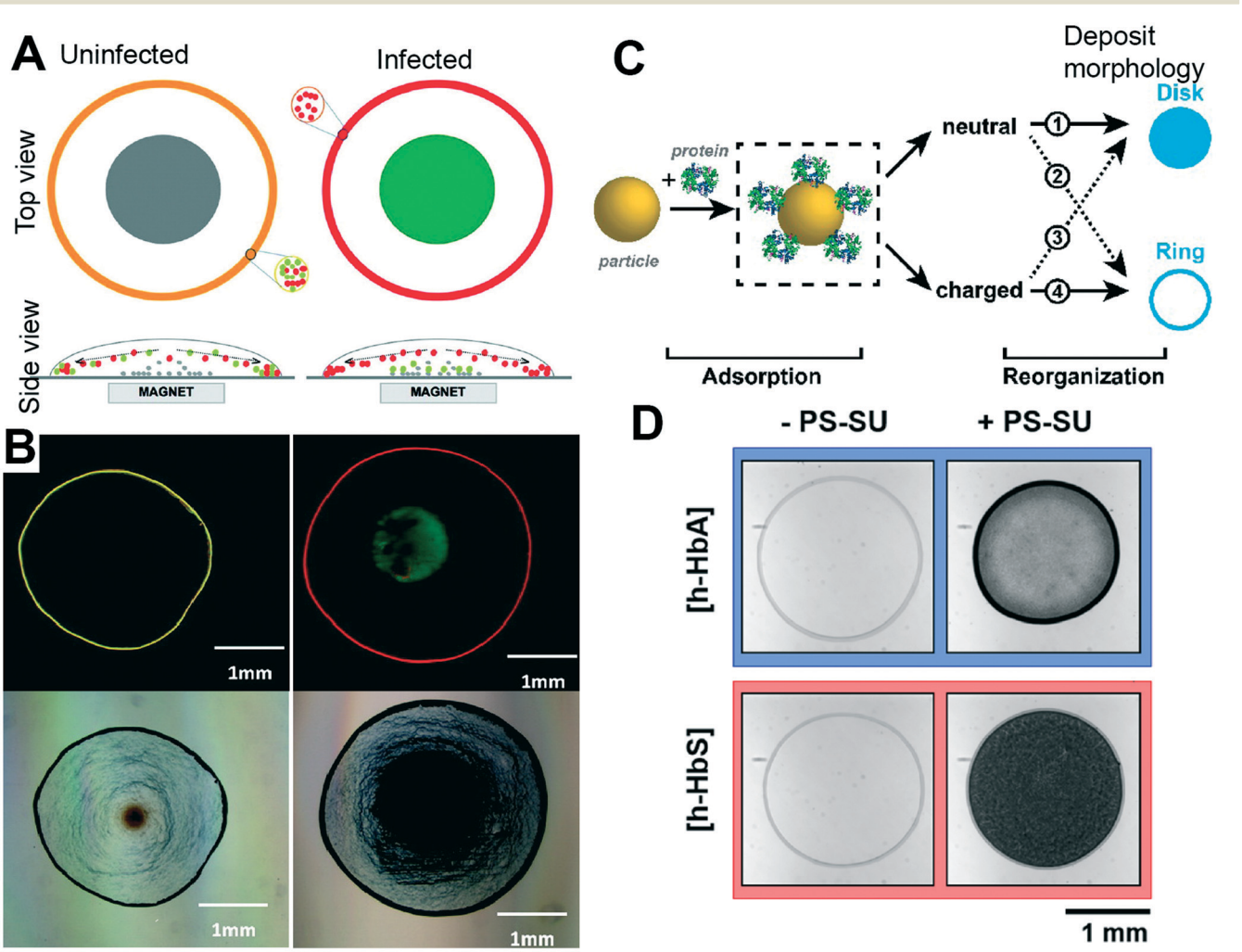

Fig. 7 Coffee-ring effect for disease diagnosis. (A) Biomarker indicator particles (green), magnetic particles (gray), and non-reactive control particles (red) are mixed in a droplet. In the absence of the disease biomarker, both colored particles are transported to the rim of the droplet as it evaporates, and combine to give a yellowish color to the coffee-ring. When the biomarker is present, both magnetic and indicator particles cross-link and are attracted to the center by the magnet, leaving a distinctive green spot. Red particles get deposited on the edge of the coffee ring. (B) Fluorescent (top) and bright-field images (bottom) of experimental results with the scheme illustrated in (A). Adapted with permission from ref. 73. Copyright 2012 American Chemical Society. (C) Charged nanoparticles can interact with proteins in different ways and produce two different types of deposits: a coffee-ring or a disk. (D) Native human hemoglobin (h-HbA) and sickle cell hemoglobin (h-HbS) interact in the absence (–PS-SU) or presence (+PS-SU) of anionic polystyrene particles with sulfate surface groups. Bright-field images of the deposit patterns resulted from their interactions. Adapted with permission from ref. 59. Copyright 2016 American Chemical Society.

containing recombinant HRPII in the presence of AuPS is spotted onto a glass slide functionalized with Ni(II)NTA. The intensity of the coffee-ring annulus—containing AuPS aggregates—is proportional to the amount of analyte present. An improved LOD of 10 pM was reported, but the signal saturated very rapidly after 100 pM. Most important from these studies is that results are easy to distinguish, even by the naked eye. The same group later reported that Marangoni flow in a droplet could be exploited to achieve higher sensitivities by concentrating the majority of colloid aggregates at the center of the droplet (stagnation points of the Marangoni flow) instead of the coffee-ring. The spot size at the center scales linearly to the biomarker concentration.[31]

In general, a solution of any protein can produce a coffee-ring pattern, but information about their concentration or type of protein is difficult to obtain by simple visual inspection. As we mentioned above, nanoparticles can self-assemble at the coffee-ring interface and one hypotheses was if the morphology of the coffee-ring could be affected by the interaction of the nanoparticles with an analyte. Mixing a sample with nanoparticles (500 nm in diameter) whose surface contained different electrical charges proved to be an effective means to detect a single amino acid change in hemoglobin,[59] as shown in Fig. 7C and D. This technique permits the differentiation of native human hemoglobin (h-HbA) from sickle cell hemoglobin (h-HbS), the responsible of sickle cell anemia. When each protein at a concentration of 15 μM was mixed with anionic polystyrene nanoparticles they formed two distinct deposit morphologies: h-HbA generated a ring pattern while h-HbS created a homogenous disk pattern. Proteins interact with nanoparticles through electrostatic and/or hydrophobic interactions, and these interactions can affect their behavior at the liquid/gas interface. These effects combined modify the deposition patterns of a drying droplet. Similar effects were employed for the detection of nucleic acids: hybridization of a target DNA to 1 μm beads functionalized with DNA probes suppresses the coffee ring while in the absence of the target DNA, the coffee ring was formed.[74]

We should point out that the coffee ring effect is a clear shift of paradigm from current microfluidic approaches because no external equipment is needed to drive the separation. This characteristic also makes droplets a unique platform for point-of-care applications. Certainly, the efficiency and throughput of sessile droplets is limited compared to the continuous microfluidic separation techniques because it is unable to process large sample volumes; however, compared to microfluidic devices there is no need for microfabricated structures in the majority of cases.

The abovementioned examples of the coffee-ring effect nevertheless set the stage for future applications where there is a need for simple and rapid devices to pre-concentrate an analyte from a few μL of a sample solution. When designed well, the coffee-ring effect can provide an easy-to-interpret visual signal that could be useful in the development of low-cost, simple-to-use, point-of-care devices. In its current form, the limits of detection offered by the coffee-ring effect are orders of magnitude greater than ELISA. One possibility to improve the overall performance is to incorporate enzymes that produce a colorimetric signal. These enzymes could be included with the sample or added after the coffee ring is produced. As we have reviewed, Raman spectroscopy is one of the few techniques that have harnessed the properties of the coffee-ring to enhance assay sensitivity, but we believe other techniques could benefit from pre-concentration of the analytes as well.

Cell culture and cell-based assays in droplets

Maintaining and growing cells *in vitro* is one of the cornerstones of cell biology.[75] Conventional cell culture is carried out in Petri dishes, although the preferred platforms for high-throughput cell assays, including drug screening, are the 96-well or 384-well plates.[76] For drug screening systems, these microplates can be interfaced with robotic stations to increase throughput and enable automation.[77] However, volume consumption has become the largest issue with this platform and difficult to adapt for single cell culture.[76] Thus, there is a need to develop accurate, robust, and scalable alternative platforms.

As mentioned above, sessile droplets can be operated with regular pipettes and potentially interfaced to instrumentation employed for microplates. However, evaporation can alter the concentration of cell culture media that can lead to detrimental effects. To prevent evaporation, a substrate can be initially flooded in oxygen-permeable biocompatible oils (*e.g.*, mineral or silicon oil).[78] Using a standard pipette, a cell suspension is deposited on the surface under the barrier oil, forming well-defined droplets, as shown in Fig. 8A, making possible cell attachment and co-culture of two types of cells. Culture of single cells in nL-volume droplets deposited with an inkjet printer has also been demonstrated.[79] Fang and his colleagues improved this technology by patterning microwells in glass and PDMS.[77,80] After the device is immersed in oil, solutions are loaded into the microwells using a tapered capillary connected to a syringe pump. This technique, called sequential operational array (SODA), is very interesting for cell-based drug combination screening because it allows the manipulation of the droplet contents by transferring, indexing, splitting, fusion, metering, aspiration, deposition, and mixing.[81] A microfluidic pipet chip was developed to perform similar operations.[76] Using SODA with a polydimethylsiloxane (PDMS) chip, they carried out a drug-screening assay on lung cancer cells,[77] as shown in Fig. 8D. By replacing the cell culture medium every day, these authors showed that it is possible to culture cells for up to 11 days in 500 nL droplets. An improved version of this platform was developed to perform cell migration assays. The platform consisted of a 20-μm-thick polycarbonate porous membrane sandwiched between two PDMS layers, each containing an array of through-holes of 1–15 mm diameter.[80] Droplets containing reagents and/or cells on either side of the device are interconnected through

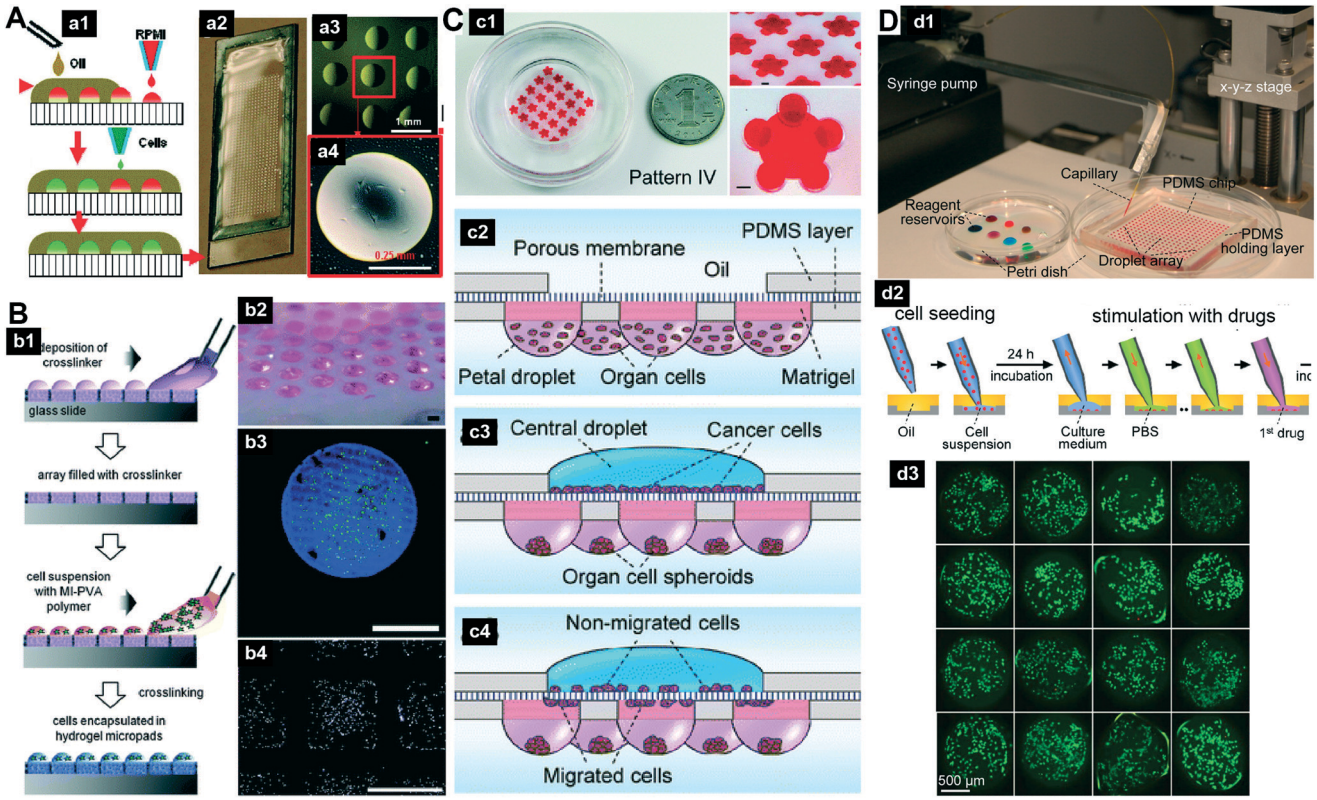

Fig. 8 Examples of cell culture and cell-based assays in sessile droplets. (A). (a1) Droplets of cell-culture medium are inkjet-printed on a glass slide, overlaid with oil, and then cells inkjet-printed; (a2) photo of the printed array on a glass slide; (a3) close-up image of 9 droplets and (a4) 1 droplet containing cells after several days of culture. Adapted with permission from ref. 79. Copyright 2011 American Chemical Society. (B). (b1) The "DropletMicroarray" facilitates the formation of hydrogel pads that encapsulate a cell suspension. (b2) A photo of the micropad array stained with a dye. (b3) Image of eGFP transfected cells inside a micropad. (b4) DAPI-stained cells after 6 days of culture. Reproduced from ref. 82 with permission from The Royal Society of Chemistry. (C). (c1) Photograph of a cell-based assay device that comprises an upper central droplet with a large volume connected through a porous membrane to five small droplets. (c2) A cell migration assay starts by generating organ cell droplets on a Matrigel layer. (c3) After organoids are formed, cancer cells are seeded on the top droplet. (c4) Some cells will migrate to the bottom layer through the membrane. Reproduced from ref. 80 with permission from The Royal Society of Chemistry. (D). (d1) Photograph of the sequential operational droplet array (SODA). (d2) Schematic of some steps in a drug combination assay that involves operations with a capillary. (d3) Representative images of a drug-screening assay performed on lung cancer cells cultured in droplets. Adapted with permission from ref. 77. Copyright 2013 American Chemical Society.

the porous membrane, as shown in Fig. 8C. With this setup, Fang and his colleagues demonstrated cell culture (up to 2 days without changing the medium), 3D culture, cell co-culture, different cell migration assays.[80]

To facilitate automation and speed assay times, the "DropletMicroarray" platform was devised with the purpose to create arrays of thousands of droplets from 700 pL to 3 μL volumes in a matter of seconds,[82] as shown in Fig. 8B. These droplets can encapsulate adherent and non-adherent cells. The platform consists of a superhydrophilic porous polymer that can be rendered superhydrophobic by exposing it to UV light through a mask. A solution dragged along the surface leads to the spontaneous formation of droplets on the hydrophilic islands, in which cells can be cultured for up to 8 hours in a high-humidity environment, without the need to use oil.

Integrating downstream analysis is essential for high-throughput applications.[83] To this end, the contents of single and multiple cells captured in droplets have been analyzed by different techniques. For example, some metabolites and membrane lipids can be analyzed by electrospray ionization mass spectrometry (ESI-MS) directly from a droplet.[83,84] While the protein content of a laser-lysed cell can be analyzed in a 10 nL droplet using a fluorescent sandwich immunoassay.[85]

Culture of single and multiple cells for several days has been demonstrated in droplets down to the nL scale, which is 2–3 orders of magnitude volume reduction compared to traditional cell culture techniques.[77] For high-throughput applications, the droplet platform could be interfaced with traditional robotic dispensing systems, non-contact printing techniques, and plate-readers. Another major advantage of this platform is that droplets are accessible for further studies or assays, even when covered by a layer of oil.

Nucleic acid amplification in sessile droplets

Nucleic acid amplification is traditionally performed in tubes or in microwell plates.[86] Although ideal for applications with

an initial high amount of DNA material, they have several limitations when working with low-volume samples, including large dead volumes and template adsorption to the walls. For example, performing single-cell methylation analysis in tubes is prone to a partial recovery of cell nucleus, decreased amplification efficiency, loss of DNA during various steps, among other causes.[86] While some microfluidic devices can perform genetic analysis on single cells, they are operated with specialized instrumentation and access to individual chambers for manipulation is difficult. In addition, these devices are fabricated in state-of-the-art cleanrooms at a high-cost with time-demanding techniques.[86,87] Sessile droplets offer a very simple and inexpensive alternative to implement different nucleic acid amplification methods with less demanding instrumentation.

Mann *et al.* implemented PCR in 1 μL droplets using as little as 32 pg of cDNA. A glass slide was patterned with 60 circular patches (1.6 mm in diameter) of hydrophobic and hydrophilic regions, each capable of holding volumes from 0.5 μL to 1.65 μL. The template was pipetted first on the slide, followed by the addition of the PCR mix, and finally overlaid with 5 μL of oil; all of these steps used only a regular pipette.[88] PCR products were analyzed off-chip in a polyacrylamide gel. Schumacher *et al.* used this slide to profile DNA methylation in single cells deposited on the circular regions.[86] Preparation, manipulation and handling of this slide is as simple as placing a slide in a regular thermocycler. This slide is commercially available from Ampligrid (Beckman Coulter).

Real-time reverse transcription PCR (qRT-PCR) has also been demonstrated on 500 nL droplets with a dynamic range of 10^3 to 10^9 microRNA copies per reaction. Fluorescence from each droplet was tracked using a fluorescence stereoscope.[89] Yu *et al.* also successfully demonstrated quantitative real-time PCR on mineral oil droplets with a volume less than 1 nL. They employed an ink-jet dispenser to speed the droplet deposition, facilitating automation and increasing throughput.[87] These authors stated that their chip compares well with a conventional PCR but requiring 120 times less reagent. Yao and colleagues analyzed the gene expression of single cells captured on a droplet employing qRT-PCR.[90] Cells are first heat-lysed, followed by subsequent addition of the RT mix and PCR mix, before being detected by a fluorescent microscope system, as shown in Fig. 9A. More recently, droplets were used to capture single cells, which were then lysed and analyzed for gene expression employing qRT-PCR.[90] A similar approach was undertaken to perform whole genome amplification (WGA) from single cells employing multiple displace amplification (MDA), as shown in Fig. 9B and C.[10]

Digital PCR has also been implemented on droplets in the nL range.[91] To generate thousands of droplets, fluid flowing through a capillary is dragged onto an array of hydrophilic micropillars, which adheres to the top of the pillar, forming droplets of different volumes (1.2 to 150 nL). This technique, called surface-assisted multifactor fluid segmentation (SAMFS), can create droplets at a rate of 50 droplets per s.[91]

Instead of employing electrical heaters or benchtop thermocyclers as discussed above, droplets can be heated employing light from a 1460 nm infrared (IR) laser.[92] Nanoliter droplets were first contact-printed with a regular pipette on a polystyrene Petri dish. To perform a PCR assay, each droplet was then laser-heated with powers of 25 mW for annealing/extension and 50 mW for melting, in 10 second cycles. Interestingly, although polystyrene tends to deform at temperatures >70 °C, the small contact area of the droplets did not damage the surface. Advantages of the IR laser include its fast heating and cooling times and the direct heating of the PCR mix, but at the cost of having to heat one droplet at a time.

The droplet platform offers a reduction of reagent consumption of at least 120 times compared to conventional PCR assays,[87,89] making analyses much more cost-effective. Performing nucleic acid amplification in droplets also offers faster heat transfer and thermal equilibrium.[93] In addition, droplets in oil remain stable for several days as no signs of coalescing were found,[87,92] and the same oil also protects each reaction from contaminating each other.[87] As we noted, other methods such as cell lysis can be performed on the same droplets without losing or diluting biomolecules. Also, there are no dead volumes, which translate into enhanced kinetic reactions.[86] However, one issue to consider is that the majority of enzymes absorb to the water/oil interface, thus a higher concentration of polymerases is required for a successful PCR.[93] Droplets contents can be easily retrieved for further downstream analysis (*e.g.*, DNA sequencing). Finally, the instrumentation for thermal cycling and for the fluorescent readers (in the case of real-time monitoring) is considerably simplified in the sessile droplet platform, which makes them ideal for point-of-care applications or for resource-limited settings.[93]

Conclusion

The present review summarizes the different types of assays that have been adapted to the sessile droplet platform. Table 1 summarizes the most common applications for sessile droplets. Most assays performed in a microtiter plate have been transferred to the sessile droplet platform but using smaller volumes and with greater flexibility and versatility. Although the droplets are not movable, and thus the range of analysis is limited to the same location, the interesting physical phenomena that arise when a droplet evaporates compensate for this limitation, as it enables other types of applications. Droplets provide an alternative paradigm to the lab-on-a-chip philosophy yet operating in a similar volume range. Performing biochemical assays in droplets can improve assay performance, allow the processing of a large number of samples in parallel, and most importantly, there is no need for time-consuming and specialized microfabrication.[10,94] In addition, sessile droplets remain accessible at all times for downstream analysis.

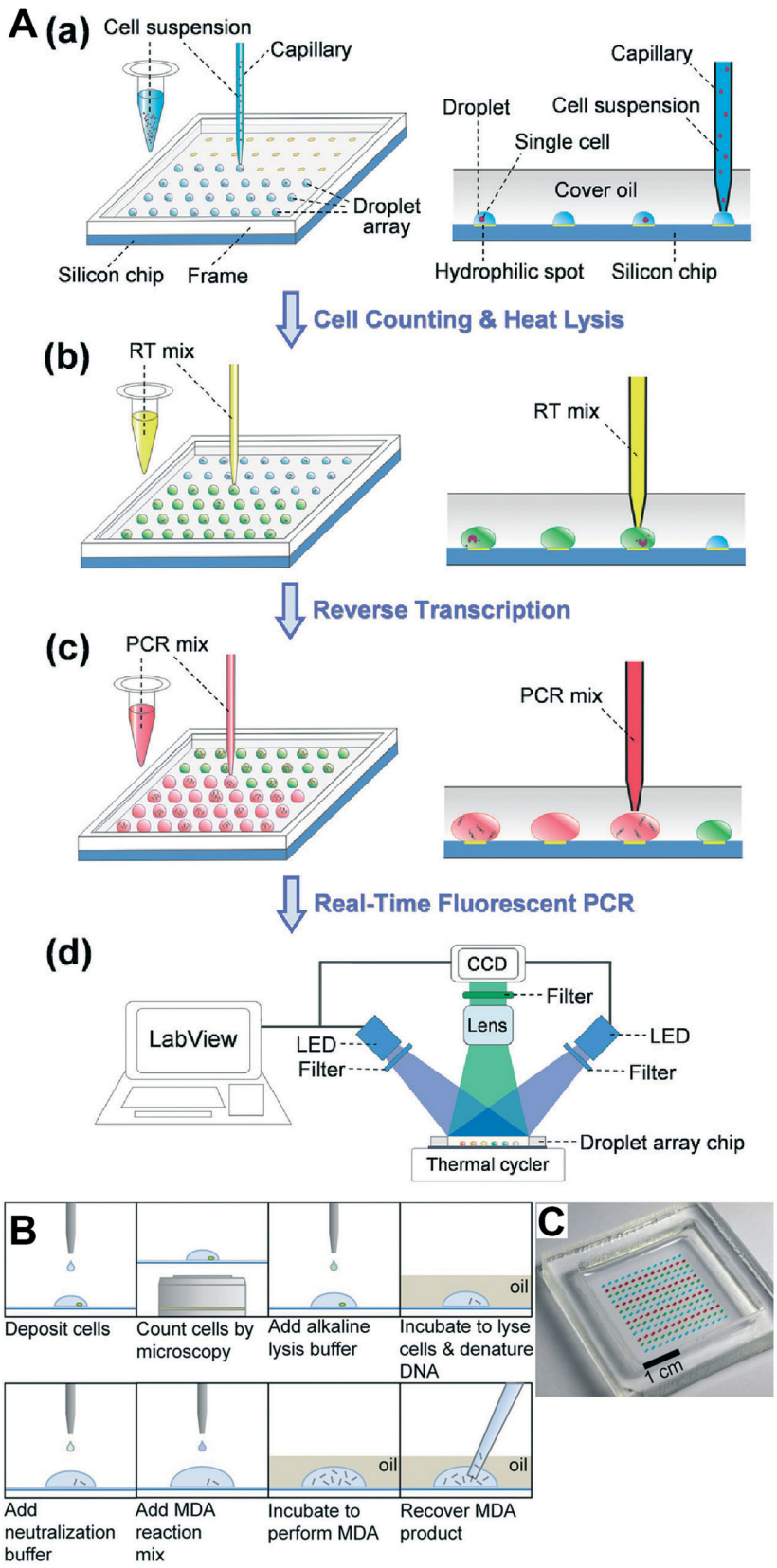

Fig. 9 Nucleic acid amplification in sessile droplets. (A) RT-PCR from single cells. A silicon chip with hydrophilic spots is initially filled with oil. (a) Single cells are deposited using a capillary and confined to these spots. (b) Heat-lysis of cells is followed by the addition of the RT mix and finally (c) the PCR mix. The droplet increases in volume as reagents are added. (d) Gene expression is monitored with a fluorescent stereoscope. Reprinted from ref. 90. (B) The process to perform an MDA assay on single cells deposited in sessile droplets. (C) Photo of the MDA platform containing 100 nL droplets. Reproduced from ref. 10, copyright 2016 Proceedings of the National Academy of Sciences.

Table 1 Applications of sessile droplets

Applications	Mechanism used	Assay examples	Assay volumes	Comments
Mixing	Marangoni flow	Colorimetric assays[8]	>1 μL	Has not been employed widely
Sample enrichment	Coffee-ring effect	Detection of different proteins, glycans, and hepatotoxins;[34,66,67] detection of antibiotics, tetracycline,[63] fluorescein[62]	0.1 to 20 μL	Width of the coffee-ring is proportional to concentration; requires special substrates for Raman spectroscopy; detection of concentrations as low as 1 μM
Sample enrichment	Evaporation	Pre-concentration of heavy metal ions,[47,48] enzymes,[49] proteins,[37–39,44,50,51] DNA,[38,41] virus,[95] and environmental pollutants[39]	>0.2 μL	Requires a super-hydrophobic surface; possible to detect single molecule with SERS and in combination with slippery liquid-infused porous surfaces (SLIPS)
Protein mutation	Coffee-ring effect and droplet evaporation	Mixing with nanoparticles to form coffee-ring for detecting mutations;[59] nano-antennas with droplet evaporation[43]	>0.8 μL	Detected in water; needs a highly concentrated solution of proteins (μM range)
Particle separation	Coffee-ring effect	Separation of red-blood cells and *E. coli* using DEP,[54] nanoparticles and microparticles,[55–58] antibodies, bacteria and cells[9]	>0.5 μL	Separations carried out often in water
Biomarker detection	Coffee-ring effect	Detection of a malaria biomarker,[72,73] thrombin in serum using a fluorescent aptamer,[64] adenovirus in human tears,[69] and nucleic acids[74]	1–3 μL	Rings visible with a naked eye, down to 10 pM in some cases
Biomarker detection	Combination of Marangoni flow and the coffee-ring effect	Detection of bacteriophages using microbeads functionalized with antibodies[31]	1 μL	Only works on PDMS or substrates with similar low-thermal conductivity
Cell-based assays	Sessile droplet	Cell culture,[76,78,82] 3D cell-culture,[80] single-cell culture,[79] drug-screening,[77,82] single-cell protein analysis,[85] cell migration[80]	10 nL to 1 μL	To avoid evaporation, droplets can be placed in a high-humidity environment, or by flooding a substrate with mineral oil
Nucleic acid amplification	Sessile droplet	PCR,[88,92,93] real-time PCR,[87] single-cell PCR,[86] RT-PCR,[89] single-cell RT-PCR,[90] digital-PCR,[91] MDA[10]	100 pL to 1 μL	Mineral oil is used to prevent evaporation

Simple and inexpensive analytical techniques are constantly sought for point-of-care devices.[9] Sessile droplets offer these attributes and other advantages, making them ideal candidates for point-of-care applications. Droplets can be highly stable, the volumes can be easily tuned, and as we have mentioned, there are multiple simple methods to produce a large number of droplets without resorting to microfluidic techniques. In addition, droplets can be potentially interfaced to liquid handling units and microplate readers, which makes them an ideal platform for scientists in industry looking to migrate their assays to higher density plates and use less sample and reagent volumes. As long as the design of the sessile droplet platform conforms to one of the microwell layouts, the related instrumentation can be adapted for the sessile droplet platform.

There are several challenges and opportunities for the sessile droplet platform. As we discussed above, evaporation is a major drawback in most assays performed in a microwell plate but in some sessile droplet applications it can be exploited to drive assay reactions or to concentrate an analyte. However, it is desirable to know beforehand the type of samples to be analyzed and the concentrations looked for, because an undesirable feature of the evaporation process is the concomitant increase in the concentration of contaminants. Note that this recurring issue also takes place in other microfluidic platforms, and it has partially been solved by pretreatment (*e.g.*, cleaning-up) of samples. Another challenge is related to controlling the droplet surroundings; air current, temperature, and humidity can alter the evaporation rate of a drying droplet and possibly affect the assay outcome. One solution is to enclose the droplets in a box with controlled humidity and temperature to provide the same conditions all the time, although this could increase the cost and complexity of the instrumentation. These challenges and mitigation strategies should be considered when deciding to implement new assays using the sessile platform.

Miniaturizing common analytical laboratory techniques in the form of devices containing microfluidic channels is the predominant purview of microfluidics. Integration of these different bioanalytical techniques into autonomous monolithic devices is at the core of the lab-on-a-chip technology.[96] Sessile droplets, on the other hand, are more analogous to the way macro-scale chemical and biology laboratories operate today: manipulating samples on tubes or wells using pipettes. Both platforms have their strengths and weaknesses; research has been largely focused on microfluidic channels and movable droplets, thus we hope this review on the advantages, challenges, and opportunities of the sessile droplet platform leads to more interest in scientific community.

Acknowledgements

JLGC acknowledges funding from Mexico's CONACyT (Grants No. 256097 and FC-1132). ZHF acknowledges financial

support from National Science Foundation (DBI-1353423), Florida Department of Health (7ZK22), McJunkin Family Charitable Foundation, and University of Florida.

References

1 S. Y. Teh, R. Lin, L. H. Hung and A. P. Lee, *Lab Chip*, 2008, **8**, 198–220.
2 N. Shembekar, C. Chaipan, R. Utharala and C. A. Merten, *Lab Chip*, 2016, **16**, 1314–1331.
3 O. J. Dressler, R. M. Maceiczyk, S. I. Chang and A. J. deMello, *J. Biomol. Screening*, 2014, **19**, 483–496.
4 P. Zhu and L. Wang, *Lab Chip*, 2016, **17**, 34–75.
5 K. Choi, A. H. Ng, R. Fobel and A. R. Wheeler, *Annu. Rev. Anal. Chem.*, 2012, **5**, 413–440.
6 J. Lee and C. J. Kim, *J. Microelectromech. Syst.*, 2000, **9**, 171–180.
7 M. G. Pollack, R. B. Fair and A. D. Shenderov, *Appl. Phys. Lett.*, 2000, **77**, 1725–1726.
8 R. Hernandez-Perez, Z. H. Fan and J. L. Garcia-Cordero, *Anal. Chem.*, 2016, **88**, 7312–7317.
9 T. S. Wong, T. H. Chen, X. Shen and C. M. Ho, *Anal. Chem.*, 2011, **83**, 1871–1873.
10 K. Leung, A. Klaus, B. K. Lin, E. Laks, J. Biele, D. Lai, A. Bashashati, Y. F. Huang, R. Aniba, M. Moksa, A. Steif, A. M. Mes-Masson, M. Hirst, S. P. Shah, S. Aparicio and C. L. Hansen, *Proc. Natl. Acad. Sci. U. S. A.*, 2016, **113**, 8484–8489.
11 P. Banks, *Drug Discovery World*, 2009, **10**, 85–90.
12 T. S. M. Team, *Microplate Technology Usage and Trends*, http://www.the-scientist.com/?articles.view/articleNo/40906/title/Microplate-Technology-Usage-and-Trends/, (accessed 19/03/2017, 2017).
13 J. J. Burbaum, *Drug Discovery Today*, 1998, **3**, 313–322.
14 Global Industry Analysts, *Microplate instrumentation and supplies - A global strategic business report*, http://www.strategyr.com/MarketResearch/Microplate_Instrumentation_and_Supplies_Market_Trends.asp, (accessed 18/03/2017, 2017).
15 L. M. Mayr and P. Fuerst, *J. Biomol. Screening*, 2008, **13**, 443–448.
16 J. Comley, *Drug Discovery World*, 2008, **9**, 35–46.
17 E. Mitre, M. Schulze, G. A. Cumme, F. Rossler, T. Rausch and H. Rhode, *J. Biomol. Screening*, 2007, **12**, 361–369.
18 D. N. Gosalia and S. L. Diamond, *Proc. Natl. Acad. Sci. U. S. A.*, 2003, **100**, 8721–8726.
19 R. G. Larson, *AIChE J.*, 2014, **60**, 1538–1571.
20 H. Y. Erbil, *Adv. Colloid Interface Sci.*, 2012, **170**, 67–86.
21 A. M. Cazabat and G. Guena, *Soft Matter*, 2010, **6**, 2591–2612.
22 Y. Yuan and T. R. Lee, in *Surface Science Techniques*, ed. G. Bracco and B. Holst, Springer Berlin Heidelberg, Berlin, Heidelberg, 2013, pp. 3–34, DOI: 10.1007/978-3-642-34243-1_1.
23 H. Y. Erbil, G. McHale and M. I. Newton, *Langmuir*, 2002, **18**, 2636–2641.
24 C. Y. Lee and W. K. In, *J. Nucl. Sci. Technol.*, 2014, **51**, 448–456.
25 H. Hu and R. G. Larson, *Langmuir*, 2005, **21**, 3963–3971.
26 R. D. Deegan, O. Bakajin, T. F. Dupont, G. Huber, S. R. Nagel and T. A. Witten, *Nature*, 1997, **389**, 827–829.
27 R. D. Deegan, O. Bakajin, T. F. Dupont, G. Huber, S. R. Nagel and T. A. Witten, *Phys. Rev. E: Stat. Phys., Plasmas, Fluids, Relat. Interdiscip. Top.*, 2000, **62**, 756–765.
28 F. Girard, M. Antoni, S. Faure and A. Steinchen, *Langmuir*, 2006, **22**, 11085–11091.
29 H. Hu and R. G. Larson, *J. Phys. Chem. B*, 2006, **110**, 7090–7094.
30 H. Hu and R. G. Larson, *Langmuir*, 2005, **21**, 3972–3980.
31 J. R. Trantum, M. L. Baglia, Z. E. Eagleton, R. L. Mernaugh and F. R. Haselton, *Lab Chip*, 2014, **14**, 315–324.
32 S. K. Cho, Y. Zhao and C. J. Kim, *Lab Chip*, 2007, **7**, 490–498.
33 G. M. Walker and D. J. Beebe, *Lab Chip*, 2002, **2**, 57–61.
34 R. A. Halvorson and P. J. Vikesland, *Environ. Sci. Technol.*, 2011, **45**, 5644–5651.
35 C. Zhao, Z. Ge and C. Yang, *Micromachines*, 2017, **8**, 28.
36 J. L. Garcia-Cordero and S. J. Maerkl, *Lab Chip*, 2014, **14**, 2642–2650.
37 R. A. Wallace, J. J. Charlton, T. B. Kirchner, N. V. Lavrik, P. G. Datskos and M. J. Sepaniak, *Anal. Chem.*, 2014, **86**, 11819–11825.
38 F. De Angelis, F. Gentile, F. Mecarini, G. Das, M. Moretti, P. Candeloro, M. L. Coluccio, G. Cojoc, A. Accardo, C. Liberale, R. P. Zaccaria, G. Perozziello, L. Tirinato, A. Toma, G. Cuda, R. Cingolani and E. Di Fabrizio, *Nat. Photonics*, 2011, **5**, 683–688.
39 S. Yang, X. Dai, B. B. Stogin and T. S. Wong, *Proc. Natl. Acad. Sci. U. S. A.*, 2016, **113**, 268–273.
40 J. L. Garcia-Cordero, C. Nembrini, A. Stano, J. A. Hubbell and S. J. Maerkl, *Integr. Biol.*, 2013, **5**, 650–658.
41 A. Ebrahimi, P. Dak, E. Salm, S. Dash, S. V. Garimella, R. Bashir and M. A. Alam, *Lab Chip*, 2013, **13**, 4248–4256.
42 A. Accardo, E. Trevisiol, A. Cerf, C. Thibault, H. Laurell, M. Buscato, F. Lenfant, J.-F. Arnal, C. Fontaine and C. Vieu, *J. Vac. Sci. Technol., B: Nanotechnol. Microelectron.: Mater., Process., Meas., Phenom.*, 2016, **34**, 06K201.
43 M. L. Coluccio, F. Gentile, G. Das, A. Nicastri, A. M. Perri, P. Candeloro, G. Perozziello, R. Proietti Zaccaria, J. S. Gongora, S. Alrasheed, A. Fratalocchi, T. Limongi, G. Cuda and E. Di Fabrizio, *Sci. Adv.*, 2015, **1**, e1500487.
44 F. Gentile, M. L. Coluccio, N. Coppede, F. Mecarini, G. Das, C. Liberale, L. Tirinato, M. Leoncini, G. Perozziello, P. Candeloro, F. De Angelis and E. Di Fabrizio, *ACS Appl. Mater. Interfaces*, 2012, **4**, 3213–3224.
45 T. S. Wong, S. H. Kang, S. K. Tang, E. J. Smythe, B. D. Hatton, A. Grinthal and J. Aizenberg, *Nature*, 2011, **477**, 443–447.
46 P. Dak, A. Ebrahimi and M. A. Alam, *Lab Chip*, 2015, **15**, 931–931.
47 I. Yanagimachi, N. Nashida, K. Iwasa and H. Suzuki, *Sci. Technol. Adv. Mater.*, 2005, **6**, 671–677.
48 I. Yanagimachi, N. Nashida, K. Iwasa and H. Suzuki, *IEEJ Trans. Electr. Electron. Eng.*, 2009, **4**, 365–371.
49 M. Hashimoto, N. Sakamoto, S. Upadhyay, J. Fukuda and H. Suzuki, *Biosens. Bioelectron.*, 2007, **22**, 3154–3160.

50 M. L. McLauchlin, D. Q. Yang, P. Aella, A. A. Garcia, S. T. Picraux and M. A. Hayes, *Langmuir*, 2007, **23**, 4871–4877.
51 J. McLane, C. Wu and M. Khine, *Adv. Mater. Interfaces*, 2015, **2**, 1400034.
52 J. McGrath, M. Jimenez and H. Bridle, *Lab Chip*, 2014, **14**, 4139–4158.
53 P. Sajeesh and A. K. Sen, *Microfluid. Nanofluid.*, 2014, **17**, 1–52.
54 J. Y. Jung and H. Y. Kwak, *Anal. Chem.*, 2007, **79**, 5087–5092.
55 J. Y. Jung, Y. W. Kim and J. Y. Yoo, *Anal. Chem.*, 2009, **81**, 8256–8259.
56 J. Y. Jung, Y. W. Kim, J. Y. Yoo, J. Koo and Y. T. Kang, *Anal. Chem.*, 2010, **82**, 784–788.
57 C. Monteux and F. Lequeux, *Langmuir*, 2011, **27**, 2917–2922.
58 C. C. Wong, Y. X. Liu, K. Y. Wang and A. R. A. Rahman, *Lab Chip*, 2013, **13**, 3663–3667.
59 S. Devineau, M. Anyfantakis, L. Marichal, L. Kiger, M. Morel, S. Rudiuk and D. Baigl, *J. Am. Chem. Soc.*, 2016, **138**, 11623–11632.
60 H. Erwin and B. G. Yogesh, *J. Micromech. Microeng.*, 2013, **23**, 075016.
61 Y. Liu, C. Z. Huang and Y. F. Li, *Anal. Chem.*, 2002, **74**, 5564–5568.
62 Y. Liu, Y. F. Li and C. Z. Huang, *J. Anal. Chem.*, 2006, **61**, 647–653.
63 C. Z. Huang, Y. Liu and Y. F. Li, *J. Pharm. Biomed. Anal.*, 2004, **34**, 103–114.
64 J. T. Wen, C. M. Ho and P. B. Lillehoj, *Langmuir*, 2013, **29**, 8440–8446.
65 C. L. Haynes, A. D. McFarland and R. P. V. Duyne, *Anal. Chem.*, 2005, **77**, 338 A–346 A.
66 D. Zhang, Y. Xie, M. F. Mrozek, C. Ortiz, V. J. Davisson and D. Ben-Amotz, *Anal. Chem.*, 2003, **75**, 5703–5709.
67 J. Filik and N. Stone, *Analyst*, 2007, **132**, 544–550.
68 E. Kočišová and M. Procházka, *J. Raman Spectrosc.*, 2011, **42**, 1606–1610.
69 S. Choi, S. W. Moon, J. H. Shin, H. K. Park and K. H. Jin, *Anal. Chem.*, 2014, **86**, 11093–11099.
70 W. D. Wang, Y. G. Yin, Z. Q. Tan and J. F. Liu, *Nanoscale*, 2014, **6**, 9588–9593.
71 X. Y. Shen, C. M. Ho and T. S. Wong, *J. Phys. Chem. B*, 2010, **114**, 5269–5274.
72 C. P. Gulka, J. D. Swartz, J. R. Trantum, K. M. Davis, C. M. Peak, A. J. Denton, F. R. Haselton and D. W. Wright, *ACS Appl. Mater. Interfaces*, 2014, **6**, 6257–6263.
73 J. R. Trantum, D. W. Wright and F. R. Haselton, *Langmuir*, 2012, **28**, 2187–2193.
74 Y. H. Li, Z. C. Zhao, M. L. Lam, W. Liu, P. P. Yeung, C. C. Chieng and T. H. Chen, *Sens. Actuators, B*, 2015, **206**, 56–64.
75 M. Mehling and S. Tay, *Curr. Opin. Biotechnol.*, 2014, **25**, 95–102.
76 Y. Zhou, Y. Pang and Y. Huang, *Anal. Chem.*, 2012, **84**, 2576–2584.
77 G. S. Du, J. Z. Pan, S. P. Zhao, Y. Zhu, J. M. den Toonder and Q. Fang, *Anal. Chem.*, 2013, **85**, 6740–6747.
78 E. Luong-Van, R. K. Kang and W. R. Birch, *Biointerphases*, 2009, **4**, 13–18.
79 A. R. Liberski, J. T. Delaney and U. S. Schubert, *ACS Comb. Sci.*, 2011, **13**, 190–195.
80 Y. Ma, J.-Z. Pan, S.-P. Zhao, Q. Lou, Y. Zhu and Q. Fang, *Lab Chip*, 2016, **16**, 4658–4665.
81 Y. Zhu, Y. X. Zhang, L. F. Cai and Q. Fang, *Anal. Chem.*, 2013, **85**, 6723–6731.
82 E. Ueda, F. L. Geyer, V. Nedashkivska and P. A. Levkin, *Lab Chip*, 2012, **12**, 5218–5224.
83 X. C. Zhang, Z. W. Wei, X. Y. Gong, X. Y. Si, Y. Y. Zhao, C. D. Yang, S. C. Zhang and X. R. Zhang, *Sci. Rep.*, 2016, **6**, 24730.
84 S. R. Ellis, C. J. Ferris, K. J. Gilmore, T. W. Mitchell, S. J. Blanksby and M. in het Panhuis, *Anal. Chem.*, 2012, **84**, 9679–9683.
85 A. Salehi-Reyhani, E. Burgin, O. Ces, K. R. Willison and D. R. Klug, *Analyst*, 2014, **139**, 5367–5374.
86 M. Kantlehner, R. Kirchner, P. Hartmann, J. W. Ellwart, M. Alunni-Fabbroni and A. Schumacher, *Nucleic Acids Res.*, 2011, **39**, e44.
87 Y. N. Sun, X. G. Zhou and Y. D. Yu, *Lab Chip*, 2014, **14**, 3603–3610.
88 U. Schmidt, S. Lutz-Bonengel, H. J. Weisser, T. Sanger, S. Pollak, U. Schon, T. Zacher and W. Mann, *Z. Rechtsmed.*, 2006, **120**, 42–48.
89 Y. Zhang, Y. Zhu, B. Yao and Q. Fang, *Lab Chip*, 2011, **11**, 1545–1549.
90 Y. Zhu, Y. X. Zhang, W. W. Liu, Y. Ma, Q. Fang and B. Yao, *Sci. Rep.*, 2015, **5**, 9551.
91 W. W. Liu, Y. Zhu, Y. M. Feng, J. Fang and Q. Fang, *Anal. Chem.*, 2017, **89**, 822–829.
92 H. Kim, S. Vishniakou and G. W. Faris, *Lab Chip*, 2009, **9**, 1230–1235.
93 S. L. Angione, A. Chauhan and A. Tripathi, *Anal. Chem.*, 2012, **84**, 2654–2661.
94 K. T. Kotz, K. A. Noble and G. W. Faris, *Appl. Phys. Lett.*, 2004, **85**, 2658–2660.
95 S. Yang, P. J. Hricko, P.-H. Huang, S. Li, Y. Zhao, Y. Xie, F. Guo, L. Wang and T. J. Huang, *J. Mater. Chem. C*, 2014, **2**, 542–547.
96 I. K. Dimov, L. Basabe-Desmonts, J. L. Garcia-Cordero, B. M. Ross, A. J. Ricco and L. P. Lee, *Lab Chip*, 2011, **11**, 845–850.

